Transit times of radiation through photonic bandgap materials: Pulse reshaping of classical and quantum fields in the time domain

Martin Ligare*
Department of Physics, Bucknell University, Lewisburg, PA 17837

Aaron Gee-Clough
Department of Physics and Astronomy, University College London, London, England WC1E 6BT†

Charles Doersam
Department of Physics, Lycoming College, Williamsport, PA 17701
(Dated: October 21, 2002)

We study the propagation of model electromagnetic pulses through photonic bandgap materials and relate time-domain pulse reshaping to observable transit times. For layered dielectric mirrors we demonstrate how pulse reshaping of slowly varying classical fields results in transit-time delays that are equivalent to the group delay. The time-domain analysis emphasizes the causal origin of negative group delays. We also study an analogous fully-quantized model and show how the same time-domain analysis may be used to interpret observed delays of single-photon fields.

PACS numbers: 03.65.Xp, 42.25.Bs, 42.50.-p, 42.70.Qs

I. INTRODUCTION

The propagation speed of particles through tunneling regions has been studied theoretically since the early days of quantum mechanics, and optical analogs of tunneling have been explored in recent years because of their experimental accessibility. The physical meaning of group velocities greater than the vacuum speed of light c has been investigated in experimental work on the propagation of photons through layered dielectric materials with photonic bandgaps at the frequency of the light [1–3]. The measured delays of individual photons in these experiments were consistent with the group delay calculated as the derivative of the phase of the transmission amplitude with respect to angular frequency. The group delay can be negative, seemingly consistent with propagation at a speed greater than c. As has been pointed out previously these anomalous delays are the result of pulse reshaping and they do not imply a violation of Einstein causality [1–3].

In this paper we take advantage of the regularity of layered dielectric mirrors to explore explicit effects of pulse reshaping in the time domain on idealized model pulses, and we use this framework to interpret the origin of the observed pulse delays. We study reshaping of both classical field pulses and fully-quantized single-photon "pulses." We make a quantitative connection between the time-domain reshaping and the conventional group delay that yields insight into the origin of observed negative delays. (Experimentally, the time-domain detection of "superluminal" optical pulses is difficult, but such studies are possible in the terahertz [4] and microwave [5] regions of the electromagnetic spectrum, and analogous acoustic waves that travel faster than the speed of sound are experimentally accessible [6].) Our time-domain analysis is a specific example of the "interference between ... causally propagating consecutive components" that was proposed as universal mechanism for understanding delays in nondissipative media in Ref. [7], and we extend the classical ideas of Ref. [7] into the domain of quantum mechanics and the transmission of single photons. Our analysis is complementary to analyses in the frequency domain like that of Ref. [8].

We consider propagation through mirrors comprised of layers of non-dispersive linear dielectric materials, each of which can be characterized by a single real index of refraction n_i. This means that within a single material electromagnetic waves propagate with equal phase and group velocities given by c/n_i. The reduced speeds within such materials are partially responsible for observed pulse delays, but the reshaping due to multiple reflections also plays a significant role. Analogous anomalous sound speeds due to pulse reshaping in one-dimensional acoustic bandgaps have also been investigated experimentally [6].

We study propagation of plane waves which are normally incident on layered dielectrics; the thickness of a layer is given by d_i and the index by n_i. To keep things simple we limit the analysis to materials in which the optical path length is the same for all layers, which means that the time it takes light to cross a layer is the same for all layers. For convenience we define a time δ_A which is the round trip time within a layer, i.e., twice the transit time,

$$\delta_A = \frac{2d_i n_i}{c}, \tag{1}$$

which is independent of the index i. We also define a time δ_B which corresponds to the delay of a wavefront

*mligare@bucknell.edu
†Current Address: 102 Parkside Rd, Silver Spring, MD, 20910

propagating through the entire mirror:

$$\delta_B = \frac{1}{c}\sum_i d_i(n_i - 1). \tag{2}$$

In Sec.II we examine the propagation of classical fields and delineate the dependence of the observed delays on the two parameters δ_A and δ_B. In Sec. III we extend the analysis to fully-quantized single photon fields, and draw parallels between the propagation of classical and quantum fields.

II. PROPAGATION OF CLASSICAL FIELDS

Pulse reshaping in layered dielectrics is most dramatic for pulses with abrupt changes in amplitude, and we first consider the effects on square pulses. Although the reshaping of such pulses leads to significant distortion, the simplicity of square pulses makes it easy to disentangle the effects leading to transit-time delays. After demonstrating the nature of the reshaping effects with square pulses we discuss slowly varying pulses, and derive quantitative expressions for delays.

A. Reshaping of Square Pulses

We consider a classical square pulse with complex magnitude $\mathcal{E}$ and duration τ, and assume that in the absence of any dielectric material this pulse arrives at the observation point at $t = 0$, so that the observed complex field amplitude after propagating through a vacuum can be written

$$E_1(t) = \begin{cases} 0 & \text{for } t < 0 \\ \mathcal{E}e^{-i\omega t} & \text{for } 0 \le t \le \tau \\ 0 & \text{for } t > \tau \end{cases} . \tag{3}$$

When the field passes through a layered dielectric slab the field arriving at the observation point is composed of multiple reflections. The leading edge of the transmitted field undergoes no reflections, and is delayed by the time δ_B; reflected fractions of the field will be additionally delayed by multiples of δ_A. We write the total field arriving at the observation point as the sum of terms grouped according the how much time the field has spent traversing the mirror. The first term corresponds to light that suffers no reflections; the second to light that spends an "extra" time δ_A within the mirror; the third to light that spends an "extra" time $2\delta_A$ within the mirror, etc. (The terms are *not* grouped by the number of reflections. For example, some fields spending an "extra" time 2δ will have undergone two internal reflections, while some will have undergone four.) We separate the transmission coefficient for each *term* into a real factor describing the attenuation, and a complex factor giving the phase shift, so that the total field arriving at the observation point is written

$$\begin{aligned} E_2(t) \;=\; & \mathcal{E}e^{-i\omega t}\Big[\Theta(t-\delta_B)T_0 e^{i2\pi c\delta_B/\lambda} \\ & +\Theta(t-\delta_B-\delta_A)T_1 e^{i2\pi c(\delta_B+\delta_A)/\lambda} \\ & +\Theta(t-\delta_B-2\delta_A)T_2 e^{i2\pi c(\delta_B+2\delta_A)/\lambda} \\ & +\cdots\Big], \end{aligned} \tag{4}$$

where in this expression (and throughout this article) λ refers to the wavelength in vacuum. For a single dielectric layer the attenuation coefficients are

$$T_j = \frac{4n}{(n+1)^2}\left(\frac{n-1}{n+1}\right)^{2j-2}. \tag{5}$$

For more complex materials the coefficients T_i are constructed from products of the appropriate single-interface reflection and transmission coefficients.

For pulses with durations τ that are large compared to the round-trip time δ_A, many terms in Eq. (4) have time to "turn on" before the pulse completely passes by the observation point. In the middle of such pulses the effective total transmission coefficient is

$$T_{\text{total}} = \sum_j^N T_j e^{i2\pi c(\delta_B + j\delta_A)}, \tag{6}$$

where N is the number of terms that are "on" at the observation time. As N grows large the transmission approaches that given by the standard steady-state transmission coefficient, which can be expressed as

$$T_{\text{s.s.}} = \sum_j^\infty T_j e^{i2\pi c(\delta_B + j\delta_A)}. \tag{7}$$

Some examples of the effects of simple dielectric layers on square pulses are illustrated in Fig. 1. The top graph in the figure illustrates the time-dependence of the transmission through a single layer whose optical path length is $(m+1/4)\lambda$, so that $e^{i2\pi c\delta_A/\lambda} = -1$, corresponding to a minimum in the steady-state transmission. The first arrival of the transmitted pulse is delayed by δ_B, and this early arriving field is larger in magnitude than the rest of the pulse because at this time there are not yet any interference effects reducing the field. The lower graph displays transmission through a three-layer mirror. The additional layers result in an increased delay in the arrival of the leading edge and a reduction in the steady-state transmission coefficient. The additional layers also result in an enhancement of the large magnitude of the leading-edge (when compared to the steady-state transmission). The relatively large early-time transmission lasts for times on the order of δ_A, the time between arrival of fields corresponding to terms in Eq. (4). Note, though, that for multi-layer mirrors it takes more time for the effects of all of the multiple reflections to "turn on" at the observation point, and it takes longer for the transmitted pulse to settle down to the steady-state intensity.

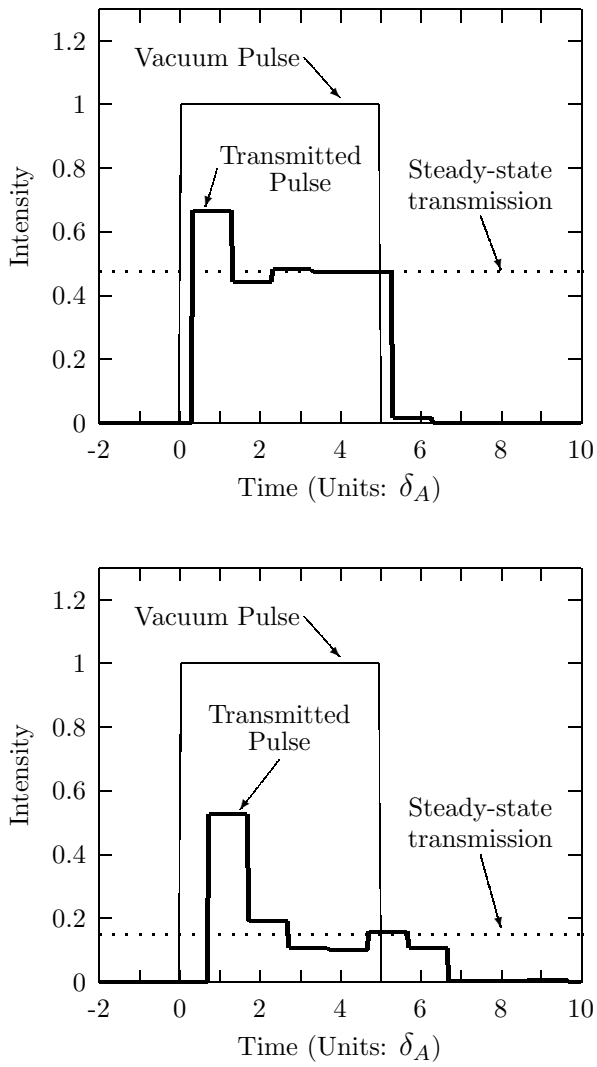

FIG. 1: Transmission of square pulse through simple dielectric slabs. The top graph is for a single layer with $n = 2.5$ and the bottom is for three layers with $n_1 = 2.5$, $n_2 = 1.25$, and $n_3 = 2.5$. In both graphs the optical path length of the dielectric layers is chosen to be $(m + 1/4)\lambda$, where m is an integer, so that the steady-state transmission is a minimum. The time units correspond to the round-trip time through a single layer, i.e., $\delta_A = 2n_i d_i/c$. The corresponding leading edge delays, δ_B, are 0.3 and 0.7 in the upper and lower graphs respectively.

The net effect of the layered dielectric is to create a transmitted field whose first arrival is delayed by δ_B, but whose temporal intensity profile is reshaped so that there is relatively more intensity at early times compared to the intensity profile of the vacuum pulse. This shifting of intensity to relatively earlier times contributes to an effective advance of the pulse. If a single arrival time is to be assigned to a pulse (or a photon), the relative role of these two effects must be accounted for when understanding seemingly anomalous velocities.

We note that for wavelengths corresponding to transmission maxima, the intensity profiles would differ from those illustrated in Fig. 1. The time of first arrival would be unchanged, but the initial field would be relatively low, and would take time to "build up" to its steady-state value. The resulting pulse profile would show relatively more intensity at later times compared to the profile of the vacuum pulse, contributing to an effective delay.

B. Transmission of slowly varying pulses

For smoothly varying pulses any reshaping effects will be much smaller than those illustrated for square pulses in the previous section, but the transmitted pulse is built up from multiple reflections in much the same way. For pulses that vary slowly enough, the transmitted pulse that is constructed in this way will have the same shape as the incident pulse. We demonstrate that the transmitted pulse may be constructed such that it is delayed or advanced relative to the vacuum pulse. (No violation of causality is implied, and the intensity of the transmitted pulse is always lower than that of the vacuum pulse.)

For simplicity we consider a portion of an incident pulse with linear amplitude modulation, and assume that the linear modulation has been in effect since a time t_0, so that the incident field can be written

$$E_1(t) = \mathcal{E}_0 \left[1 + m(t - t_0)\right] e^{-i\omega t}. \tag{8}$$

In the following analysis we assume that the round trip time within the slab is much less than the time that the modulation has been in effect, i.e., $\delta_A \ll (t - t_0)$. This means that a very large number of the terms in a series like that of Eq. (4) have "turned on," and the transmitted field is

$$\begin{aligned} E_2(t) &= \mathcal{E}_0 e^{-i\omega t} \Big\{ \left[1 + m(t - t_0 - \delta_B)\right] T_0 e^{i2\pi c\delta_B/\lambda} + \left[1 + m(t - t_0 - \delta_B - \delta_A)\right] T_1 e^{i2\pi c(\delta_B+\delta_A)/\lambda} \\ &\quad + \left[1 + m(t - t_0 - \delta_B - 2\delta_A)\right] T_2 e^{i2\pi c(\delta_B+2\delta_A)/\lambda} + \cdots \Big\} \\ &= \mathcal{E}_0 e^{-i\omega t} \sum_{j=0}^{N} \left[1 + m(t - t_0 - \delta_B - j\delta_A)\right] T_j e^{i2\pi c(\delta_B+j\delta_A)/\lambda}, \end{aligned} \tag{9}$$

where N is the number of terms that have "turned on." When N is large, the transmitted field is approximately

$$E_2(t) \simeq \mathcal{E}_0 e^{-i\omega t} T_{\rm s.s.} \left[1 + m \left(t - t_0 - \delta_B - \delta_A \frac{\sum_{j=1}^{\infty} j T_j e^{i2\pi c(\delta_B + j\delta_A)/\lambda}}{T_{\rm s.s.}} \right) \right]. \tag{10}$$

To first order in the small quantity $\delta_A/(t - t_0 - \delta_B)$ the transmitted field is

$$E_2(t) \simeq \mathcal{E}_0 e^{-i(\omega t + \alpha)} T_{\rm s.s.} \left\{ 1 + m \left[t - t_0 - \delta_B - \delta_A {\rm Re} \left(\frac{\sum_{j=1}^{\infty} j T_j e^{i2\pi c(\delta_B + j\delta_A)/\lambda}}{T_{\rm s.s.}} \right) \right] \right\}, \tag{11}$$

where α is a phase shift that will not be of further consequence in this analysis.

Comparing the expression for the transmitted field given by Eq. (11) to that of the incident field, Eq. (8), shows that the net result of the multiple reflections is an effective time delay of the linearly changing field given by

$$\delta_{\rm effective} = \delta_B + \delta_A {\rm Re} \left(\frac{\sum_{j=1}^{\infty} j T_j e^{i2\pi c(\delta_B + j\delta_A)/\lambda}}{T_{\rm s.s.}} \right). \tag{12}$$

This effective delay can be positive, corresponding to a true delay, or it can be negative, corresponding to an advance. The exact value of the delay depends on the indices of refraction in the material comprising the mirror and the number of layers in the mirror.

The first term in Eq. (12), δ_B, is simply the delay due to the reduced speed of wave-fronts within the dielectric materials. It is always a positive quantity, corresponding to an actual delay. The second term contains the more complicated effects of phased reflections, and may be positive or negative. If it is negative and greater in magnitude than δ_B, the multiple reflection effects that led to the reshaping of square pulses dominate over the effect of reduced wave-front velocity, and the total delay is negative. It is important to note that the effective time delay does not arise from the simple shifting of the incident field at a given time to a new time. Rather, the effective delay is the result of the superposition of attenuated and phase-shifted fields from many previous times.

Pulses will maintain their shapes and exhibit delays given by $\delta_{\rm effective}$ as long as the time scale characterizing the modulation is long compared to δ_A, the time between the arrival of successive reflections. The peak of the transmitted pulse may arrive after the peak of the vacuum pulse would have arrived, or before. This is because the transmitted pulse is not the result of simple attenuation of the incident peak, but rather it is constructed from the superposition of many reflections, as in Eq. (4). Slowly varying pulses are special in the sense that the newly constructed pulse has the same shape as the incident pulse. We emphasize that the effective delay does not apply to the arrival time of any feature associated with an abrupt change in the field; the arrival of the leading edge of any disturbance associated with such an abrupt change will be delayed by δ_B.

We conclude this section by demonstrating that the effective delay given by Eq. (12) is identical to that predicted by the conventional group delay, which is the derivative of the phase of the transmission amplitude with respect to angular frequency. Experimental measurements of delays have been consistent with the group delay, and our time-domain approach gives a physical picture of the origin of the observed delays.

The steady-state transmission coefficient is given by Eq. (7), and the phase of this transmission coefficient is

$$\begin{aligned} \phi &= \arctan \left[\frac{{\rm Im}(T_{\rm s.s.})}{{\rm Re}(T_{\rm s.s.})} \right] \\ &= \arctan \left[\frac{{\rm Im}(\sum_j^{\infty} T_j e^{i2\pi c(\delta_B + j\delta_A)})}{{\rm Re}(\sum_j^{\infty} T_j e^{i2\pi c(\delta_B + j\delta_A)})} \right]. \end{aligned} \tag{13}$$

It is straightforward to show that

$$\begin{aligned} \frac{d\phi}{d\omega} &= \frac{1}{\left[\left(\frac{{\rm Im}(T_{\rm s.s.})}{{\rm Re}(T_{\rm s.s.})} \right)^2 + 1 \right]} \frac{d}{d\omega} \left[\frac{{\rm Im}(T_{\rm s.s.})}{{\rm Re}(T_{\rm s.s.})} \right] \\ &= \delta_B - \delta_A {\rm Re} \left(\frac{\sum_{j=1}^{\infty} j T_j e^{i2\pi c(\delta_B + j\delta_A)/\lambda}}{T_{\rm s.s.}} \right), \end{aligned} \tag{14}$$

which is equal to $\delta_{\rm effective}$, the effective delay given by Eq. (12), which was derived above from time-domain considerations.

The equivalence (for slowly varying pulses) of the group delay with the effective delay derived in the time-domain is a further demonstration that the group delay has a physical meaning, even in cases in which it results in a seemingly anomalous advance in the peak of the transmitted pulse relative to the peak of a vacuum pulse. For pulses which vary rapidly on the time-scale given by δ_A there will be significant distortion of the shape of the pulse that will depend on the details of the pulse shape and the characteristics of the dielectric mirror. Any discussion of delays for such pulses must carefully account for such distortions in a way that is beyond the scope of the present analysis.

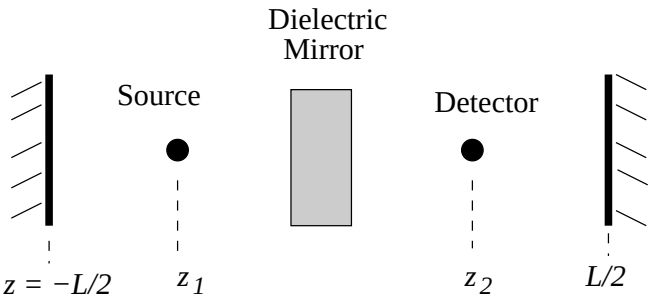

FIG. 2: Quantum model consisting of a pair of two-level atoms at fixed positions in a large multimode optical cavity. A dielectric mirror is centered in the cavity. We quantize the modes of the *inhomogeneous* cavity. The atom on the left begins in the excited state and is the source of a photon; the atom on the right serves as a detector.

III. PROPAGATION OF SINGLE-PHOTON QUANTUM FIELDS

In the preceding section we discussed the effects of layered dielectric materials on the propagation of classical fields, but the experimental determinations of propagation time cited above involved the detection of individual photons. In this section we demonstrate a way in which the time-domain picture presented for classical fields can be extended to single-photon quantum fields. We develop a model in which an excited atom spontaneously emits a quantized multimode photon, and we investigate the time-dependent probability for excitation of a detector atom located on the opposite side of a dielectric mirror from the emitting atom. The time dependent excitation probability displays interference effects that are exact analogs to those experienced by classical fields.

A. Quantum Model

We consider a large one-dimensional multimode optical cavity of total length L which contains a symmetric dielectric mirror in the center of the cavity. (See Fig. 2.) The mirror is comprised of layers of homogeneous linear dielectric like that considered in Sec. II. We find the classical standing-wave modes of the electromagnetic field in a cavity that *includes* the dielectric material, and quantize the modes of this inhomogeneous cavity.

The cavity also contains a pair two-level atoms at fixed positions z_1 and z_2 on opposite sides of the dielectric region. The atom at z_1 is initially in the excited state and spontaneously emits a photon into the quantized modes of the cavity; it serves as the source of the quantized field to be transmitted through the mirror. The atom at z_2 begins in the ground state and serves as a detector of the transmitted radiation. (It is also possible to determine equivalent information about the transmitted radiation from quantities involving field operators such as the expectation value of the intensity operator, $\langle \hat{E}^- \hat{E}^+ \rangle$ [9]. We use the excitation of a two-level atom because of the ease with which can compute this quantity to high precision in our model.)

The cavity is assumed to be large, in the sense that the length L is very much greater than the wavelength of the light emitted by the atoms, i.e., this is *not* a microcavity. The finite length L does not contribute to the physical phenomena under investigation; it simply provides a convenient quantization volume for the field modes used in our calculations.

We use a standard Hamiltonian of quantum optics to calculate the time evolution of the system, and pay particular attention to the amplitude for the atom on the right side of the cavity to be found in the excited state. We note that the effects of the spontaneously emitted photon propagate causally in this model. The explicit form of the Hamiltonian we use is [10–12]

$$\begin{aligned} H &= H_{\text{atoms}} + H_{\text{field}} + H_{\text{interaction}} \\ &= \sum_j \hbar\omega^{(\text{at})}\sigma_z^{(j)} + \sum_m \hbar\omega_m a_m^\dagger a_m \\ &\quad + \sum_{j,m} \hbar\left(g_{jm} a_m \sigma_+^{(j)} + g_{jm}^* a_m^\dagger \sigma_-^{(j)}\right), \end{aligned} \tag{15}$$

in which the atoms are labeled with the index j and the field modes with index m, and where $\omega^{(at)}$ is the zero-field resonance frequency of both atoms, ω_m is the frequency of the mth field mode, a_m and $a_m^\dagger$ are the annihilation and creation operators for the mth mode, $\sigma_+^{(j)}$, $\sigma_-^{(j)}$, and $\sigma_z^{(j)}$ are the pseudo-spin operators which act on atom j, and g_{jm} gives the coupling of the jth atom to the mth field mode. In this Hamiltonian we have made the standard electric-dipole and rotating-wave approximations.

The mode frequencies ω_m in the Hamiltonian are simply those of the classical standing wave modes of the electromagnetic field. The spatial mode functions are normalized so that the energy per photon in the quantized modes is $\hbar\omega_m$. The relative magnitudes of the coupling constants g_{jm} reflect the spatial dependence of the classical mode functions, specifically the relative magnitude of the mode functions at the positions of the two atoms. Calculation of the mode frequencies and spatial mode functions for the inhomogeneous cavity involves the solution of a classical boundary value problem. This is a straightforward process in principle, although the large number of boundaries in a multi-layer dielectric mirror leads to algebraic complexity. We used transfer matrix methods [13] (adapted to electromagnetic standing waves) and the "shooting method" [14] to determine numerically the mode frequencies.

In the limit of a large cavity we may assume that the frequencies of all atomic transitions are very much greater than the fundamental frequency of the cavity. In this limit we can make the approximation that all modes that influence the dynamics of the system are near the atomic resonance, and the atom-field coupling constants can be factored into a product of a frequency-independent con-

stant and a space-dependent coupling factor. The coupling constants g_{jm} are given in terms of the electric dipole matrix element d_j between the two levels of atom j, the effective volume of the cavity V, a mode-dependent normalization factor $\mathcal{N}_m$, and the permittivity of free space ϵ_0, by

$$\begin{aligned} g_{jm} &= \pm d_j \mathcal{N}_m \left(\frac{\omega^{(\mathrm{at})}}{2\hbar\epsilon_0 V}\right) \sin\left[k_m(L/2 - z_j)\right] \\ &= \pm \Omega_j \mathcal{N}_m \sin\left[k_m(L/2 - z_j)\right], \end{aligned} \tag{16}$$

where k_m is the wave-vector for mode m, and in the last line we have defined the quantity

$$\Omega_j = d_j \left(\frac{\omega_j^{(\mathrm{at})}}{2\hbar\epsilon_0 V}\right)^{1/2}, \tag{17}$$

which is independent of the cavity mode-frequency. For symmetrically place atoms, modes with even spatial mode functions yield coupling constants with the same sign for each atom; odd mode functions give coupling constants of opposite signs. In performing our numerical calculations we use an equal number of modes above and below the atomic resonance frequency.

The basis states for describing the system are

- $|e, g; 0\rangle$: left atom excited, right atom in ground state, no photon,
- $|g, e; 0\rangle$: right atom excited, left atom in ground state, no photon,
- $|g, g; 1_m\rangle$: both atoms in ground state, one photon in m^{th} cavity mode,

and we write the state of the system as the linear combination

$$\begin{aligned} |\psi(t)\rangle &= c_1(t)|e, g; 0\rangle + c_2(t)|g, e; 0\rangle \\ &\quad + \sum_m b_m(t)|g, g; 1_m\rangle. \end{aligned} \tag{18}$$

In all the examples in this paper the system starts in the state

$$|\psi(0)\rangle = |e, g; 0\rangle, \tag{19}$$

and we pay particular attention to the complex amplitude $c_2(t)$ for the detector atom to be found in the excited state. Although it is difficult physically to prepare a state which corresponds to our initial condition, this idealized state has the advantage that at $t = 0$ all of the energy is localized at a single point (the position of the excited atom), making causal wavefronts evolving from this state particularly easy to identify. (A visualization of the propagation of the wavefronts of the intensity of the quantum field in similar models is presented in [15, 16].)

B. Method of Solution

It is possible to find analytical solutions for the time evolution of atom-cavity systems with a single photon in simple inhomogeneous cavities [17], but the complexity of the mode structure for a cavity with a many-layered mirror makes this approach intractable. Therefore we construct numerical solutions for the coefficients $c_1(t)$, $c_2(t)$ and $b_k(t)$ of Eq. (18).

We use the time-independent Schrödinger equation to determine the energies E_q and eigenstates $|E_q\rangle$ of the *total* Hamiltonian. The time evolution of the system is then straightforward to calculate. If the system begins in state

$$\begin{aligned} |\psi(0)\rangle &= |e, g; 0\rangle \\ &= \sum_q |E_q\rangle\langle E_q|e, g; 0\rangle, \end{aligned} \tag{20}$$

then the state of the system at a later time t is given by

$$|\psi(t)\rangle = \sum_q e^{-iE_q t/\hbar}|E_q\rangle\langle E_q|e, g; 0\rangle. \tag{21}$$

Projecting Eq. (21) onto the basis states gives the the time-dependent coefficients of Eq. (18):

$$\begin{aligned} c_1(t) &= \langle e, g; 0|\psi(t)\rangle \\ &= \sum_q e^{-iE_q t/\hbar}\langle e, g; 0|E_q\rangle\langle E_q|e, g; 0\rangle \\ &= \sum_q e^{-iE_q t/\hbar}\left|\langle e, g; 0|E_q\rangle\right|^2, \end{aligned} \tag{22}$$

$$\begin{aligned} c_2(t) &= \langle g, e; 0|\psi(t)\rangle \\ &= \sum_q e^{-iE_q t/\hbar}\langle g, e; 0|E_q\rangle\langle E_q|e, g; 0\rangle, \end{aligned} \tag{23}$$

and

$$\begin{aligned} b_k(t) &= \langle g, g; 1_k|\psi(t)\rangle \\ &= \sum_q e^{-iE_q t/\hbar}\langle g, g; 1_k|E_q\rangle\langle E_q|e, g; 0\rangle. \end{aligned} \tag{24}$$

We use standard numerical matrix diagonalization routines to determine the eigenvalues and eigenvectors used in these equations. We consider systems with as many as 2,000 modes, which leads to large matrix representations of the Hamiltonian, but the the matrix is sparse. Our approach is similar to that used previously in several studies [15, 16, 18].

C. Reshaping of single photon "pulses"

The graphs of this section demonstrate the analogy between the classical field and the quantum amplitude

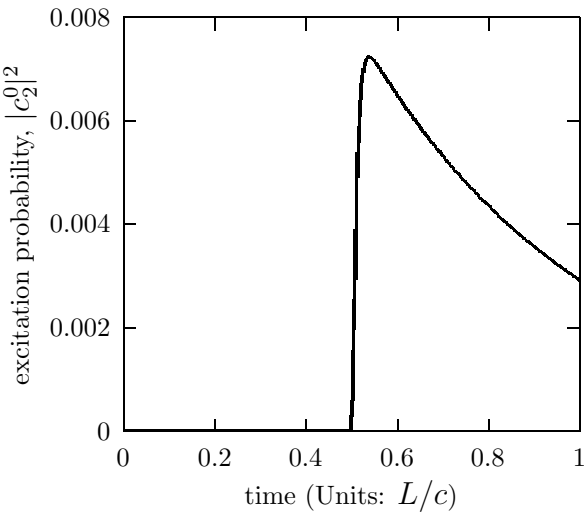

FIG. 3: Detector atom excitation probability in an empty cavity. The source atom decay rate is $\gamma_1 = 16$ and the detector atom rate is $\gamma_2 = 256$. The rapid rise at $t = 1/2$ is due to the arrival of the field at atom 2. The rate of the rise is determined by the detector response, and the slow exponential decay reflects the exponential shape of the pulse passing the detector atom.

to find the detector atom in the excited state. The total quantum amplitude is the result of interference from multiple reflections in very much the same way as the classical field is the result of multiple reflections. In this section we present results for three cavities: an empty, or vacuum cavity, a cavity with a simple homogeneous dielectric region, and a cavity containing a dielectric mirror. The results for the simple cavity help elucidate the more complicated behavior seen in the propagation of through the dielectric mirror.

For atoms in an empty cavity with no dielectric mirror it is possible to find an analytic solution for the dynamics [19]. The probability for the source atom to be in the excited state decays exponentially with decay constant $\gamma_1 = |\Omega_1|^2 L/c$ until the time at which reflections first interrupt the decay; for atomic positions $z_1 = -.25L$ and $z_2 = .25L$ this decay proceeds until reflections return to the atom time $t = 0.5L/c$. For atoms at these positions the amplitude to find the detector atom in the excited state remains identically zero until time $t = 0.5L/c$, the time at which radiation can first reach the detector. Choosing units such that $L/c = 1$ (which we will use for the remainder of the article) the amplitude to find detector atom in the excited state in an empty cavity is [19]

$$c_2^0(t) \;=\; \Theta\left(t - \frac{1}{2}\right) \frac{\sqrt{\gamma_1\gamma_2}}{\gamma_1 - \gamma_2} \times \left(e^{-\frac{\gamma_1}{2}(t-\frac{1}{2})} - e^{-\frac{\gamma_2}{2}(t-\frac{1}{2})}\right), \qquad (25)$$

in which the decay constant for the detector atom is $\gamma_2 = |\Omega_2|^2 L/c$, and the step-function expresses the turn-on of the excitation at $t = 0.5$ and the causal dynamics inherent in our model.

In the limit of very fast detector atom response, i.e., $\gamma_2 \to \infty$, the amplitude $c_2(t)$ will instantaneously reflect the strength of the field incident on the detector atom. Fig. 3 illustrates the detector atom response for the case $\gamma_1 = 16$ and $\gamma_2 = 256$. The rapid rise reflects the response of the detector atom to the sudden arrival at $t = 0.5$ of radiation from the source atom, and occurs on the time scale given by $1/\gamma_2$. The slower decline reflects the exponential shape of the radiation pulse emitted by the source as it passes by the detector atom [15, 16]. While in a given run of an actual experiment the excitation of the detector atom will be observed at a particular instant of time, the evolution of the excitation probability is continuous, and resembles the excitation expected for a classical oscillator driven by a classical field pulse.

An illustration of the effect of a single dielectric slab on a pulse is given in Fig. 4. This figure gives the time-dependence of the detector atom excitation probability after transmission of the radiation through a single dielectric slab whose width and index are chosen so that the classical delays are $\delta_A = 0.05$ and $\delta_B = 0.015$ in the units of the figure. Because the decay rate of the source atom is relatively slow, this figure is analogous to the top graph in Fig. 1, which gives the intensity of a classical square pulse after passing through a single slab of dielectric material. The excitation of the detector atom "turns on" at the expected classical time, $0.5 + \delta_B$, and is interrupted at multiples of δ_A, the classical round-trip time

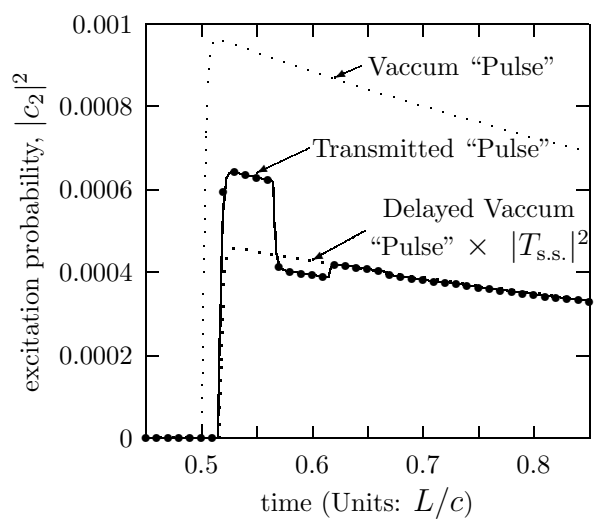

FIG. 4: Detector atom excitation probability in a cavity with a single homogeneous dielectric slab. The source atom decay rate is $\gamma_1 = 1$ and the detector atom rate is $\gamma_2 = 1024$. The width and index of the slab are chosen so that the classical delays are $\delta_A = 0.05$ and $\delta_B = 0.015$. The data points are the result of fully quantum-mechanical calculations, while the solid line is built from attenuated, delayed, and phase shifted versions of the vacuum response using *classical* delays, phase-shifts, and attenuation factors.

within the material. The excitation probability "settles down" to an attenuated and delayed version of the vacuum "pulse" of Eq. (25), where the attenuation factor is given by the *classical* $|T_{\rm s.s.}|^2$.

The data points in the figure are the result of the fully quantum mechanical calculations described in Sec. III B, while the solid line combines the quantum results for excitation in an empty cavity with the classical techniques for multiple reflections. In Sec. II the classical field is built up from a sum of appropriately attenuated, delayed, and phase shifted fields in Eq. (4); the solid line in Fig. 4 is built up from attenuated, delayed, and phase shifted versions of the quantum excitation amplitude Eq. (25) using the same *classical* attenuation, delay, and phase shift parameters that were used to produce the upper graph in Fig. 1, i.e.,

$$\text{solid line} \longleftrightarrow \Big[c_2^0(t-\delta_B)T_0 e^{i2\pi c\delta_B/\lambda} + c_2^0(t-\delta_B-\delta_A)T_1 e^{i2\pi c(\delta_A+\delta_B)/\lambda} + c_2^0(t-\delta_B-2\delta_A)T_2 e^{i2\pi c(\delta_A+2\delta_B)/\lambda} + \cdots\Big]^2. \tag{26}$$

The same principles apply to propagation through more complicated dielectric mirror structures. The excitation amplitude after transmission through an 11 element mirror with alternating high and low index regions is illustrated in Fig. 5. This mirror is similar to the $(\mathrm{HL})^5\mathrm{H}$ mirror used in the experiments of references [1, 2]. The "high" index of refraction is $n_H = 3.0$ and the "low" index is $n_L = 1.5$, giving an intensity transmission coefficient at the minimum in the transmission of $|T_{\rm s.s.}|^2 = 4.34 \times 10^{-4}$. The upper graph in this figure also shows the empty-cavity excitation probability given by the square of Eq. (25) scaled by the *classical* steady-state transmission factor, $|T_{\rm s.s.}|^2$.

The effects of the abrupt turn-on of the excitation are evident in the large variations in the early-time detection probability before the effects of multiple reflection have taken full effect. These variations are analogous to those in Figs. 1 and 4, but they last longer in this case because of the relatively large number of layers comprising the mirror. The lower graph in Fig. 5 displays the initial turn-on of the excitation of the detector atom. (Note that the vertical scale on this graph corresponds to amplitude rather than probability; the amplitude can assume negative values just as the classical field E_2 can.) As in Fig. 4, the data points are the result of the fully quantum mechanical calculations, while the solid line combines the quantum results for excitation in an empty cavity from Eq. (25) with the classical techniques for multiple reflections as in Eq. (26). There is no excitation before the time $t = 0.5 + \delta_B$, and at later times the excitation is interrupted after successive multiples of the single-layer round trip time δ_A. We call attention to the vastly different excitation probabilities at early and late times. The initial large peaks occur before the effects of multiple reflection have reduced the transmission.

The finite rise time evident in the lower graph in Fig. 5 is determined by the response of the detector atom characterized by γ_2. A more rapid detector response would show a more abrupt rise which more closely follows the step-function turn-on of the field at the detector atom. The modeling of more rapid changes would require the inclusion of more modes in our numerical analysis.

The transmission of a photon from the source through a dielectric mirror and to the detector can happen via many indistinguishable pathways: it can travel directly without undergoing reflection; it may undergo a single reflection in one of many ways, or it may undergo multiple reflections. The numerical results of this section

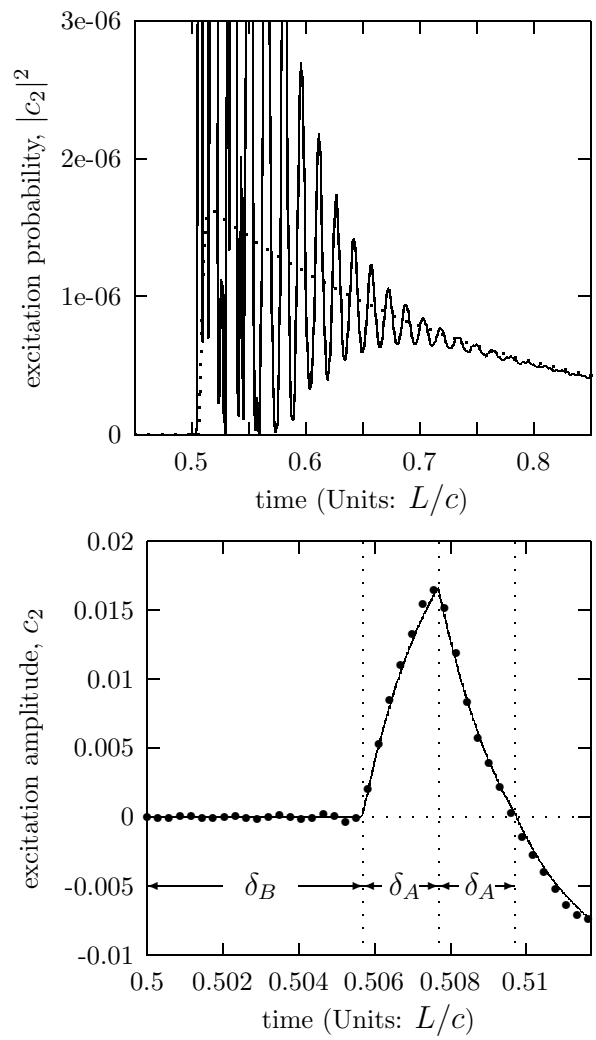

FIG. 5: Detector atom excitation in a cavity with an $(\mathrm{HL})^5\mathrm{H}$ structure dielectric mirror. The source atom decay rate is $\gamma_1 = 4$ and the detector atom rate is $\gamma_2 = 1024$. The width of the mirror elements is such that the classical delays are $\delta_A \simeq 0.002$ and $\delta_B \simeq 0.0057$. The data points are the result of fully quantum-mechanical calculations, while the solid line is built from attenuated, delayed, and phase shifted versions of the vacuum response using *classical* delays, phase-shifts, and attenuation factors. See Eq. (26).

demonstrate that the excitation amplitude for the detector atom is built up from interfering amplitudes for all of these processes in exactly the same way that the the classical transmitted field is built up from multiple reflections.

IV. CONCLUSION

We have examined the transmission of radiation through layered dielectric mirrors in the time domain. For slowly varying classical pulses we have derived a formula for pulse delays that takes into account the time-domain buildup of the steady-state transmission. The finite time that it takes to build up this steady-state transmission results in pulse reshaping, and our formula helps delineate the competing effects of pulse reshaping and the reduced front velocities in dielectric materials. The delays calculated in our model are equivalent to those calculated from the conventional group delay, but our model provides an aid to understanding and interpreting the origin of the anomalous delay times that have been observed in experiments.

We have also demonstrated that our interpretation can be extended to include quantized fields. We have studied numerically a model in which a spontaneously emitted photon propagates through a layered dielectric mirror, and excites a detector atom. The quantum amplitude to find the atom in the excited state is the result of interfering terms due to the possibility of multiple reflections in much the same way that the classical field is the result of the interference of multiply reflected fields. The terms in the quantum amplitude "turn-on" at exactly the same time as the classical field terms, and with exactly the same relative amplitudes and phases. Individual photons will be detected at a range of times described by this amplitude, and it is the distribution of arrival times of single photons that is shifted in time in exactly the same way as the classical pulse is shifted.

Acknowledgments

Two of the authors (A G.-C. and C. D.) acknowledge support from National Science Foundation Research Experiences for Undergraduates Program (Grant Number PHYS-9732158).

[1] A. M. Steinberg, P. G. Kwiat, and R. Y. Chiao, Phys. Rev. Lett. **71**, 708 (1993).
[2] A. M. Steinberg and R. Y. Chiao, Phys. Rev. A **51**, 3525 (1995).
[3] C. Spielmann, R. Szipöcs, A. Stingl, and F. Krausz, Phys. Rev. Lett. **73**, 2308 (1994).
[4] M. Reiten, K. McClatchey, D. Grischkowsky, and R. Cheville, Opt. Lett. **26**, 1900 (2001).
[5] M. Mojahedi, E. Schamiloglu, F. Hegeler, and K. J. Malloy, Phys. Rev. E **62**, 5758 (2000).
[6] W. M. Robertson, J. Ash, and J. M. McGaugh, Am. J. Phys. **70**, 689 (2002).
[7] Y. Japha and G. Kurizki, Phys. Rev. A **53**, 586 (1996).
[8] V. Romero-Rochín, R. P. Duarte-Zamorano, S. Nilsen-Hofseth, and R. G. Barrera, Phys. Rev. E **63**, 027601 (2001).
[9] L. Mandel and E. Wolf, *Optical coherence and quantum optics* (Cambridge University Press, Cambridge, 1995).
[10] P. Meystre and M. Sargent, *Elements of Quantum Optics* (Springer, Berlin, 1999), 3rd ed.
[11] M. Sargent, M. O. Scully, and W. E. Lamb, *Laser Physics* (Addison-Wesley, Reading, MA, 1974).
[12] R. Loudon, *The Quantum Theory of Light* (Oxford U. P., Oxford, 1983), 2nd ed.
[13] J. S. Walker, Comp. Phys. **6**, 393 (1992).
[14] W. H. Press, B. P. Flannery, S. A. Teukolsky, and W. T. Vetterling, *Numerical Recipes in C* (Cambridge University Press, Cambridge, 1988).
[15] M. Ligare and R. Oliveri, Am. J. Phys. **70**, 58 (2002).
[16] V. Bužek, G. Drobný, M. G. Kim, M. Havukainen, and P. L. Knight, Phys. Rev. A **60**, 582 (1999).
[17] M. Ligare, unpublished paper available at http://www.eg.bucknell.edu/phyics/ligare.html
[18] M. Ligare and S. F. Becker, Am. J. Phys. **63**, 788 (1995).
[19] T. Purdy, D. F. Taylor, and M. Ligare, arXiv:quant-ph/0204009